A new structural motif for cadmium dithiocarbamates: Crystal structures and Hirshfeld surface analyses of homoleptic zinc and cadmium morpholine dithiocarbamates

Jimmy Ahmad[I], Fiona N.-F. How[I], Siti Nadiah Abdul Halim[II], Mukesh M. Jotani[III], See Mun Lee[IV] and Edward R. T. Tiekink[*IV]

[I] Department of Chemistry, Kulliyyah of Science, International Islamic University Malaysia (IIUM), Jalan Sultan Ahmad Shah, 25200 Bandar Indera Mahkota, Kuantan, Pahang, Malaysia

[II] Department of Chemistry, University of Malaya, 50603 Kuala Lumpur, Malaysia

[III] Department of Physics, Bhavan's Sheth R. A. College of Science, Ahmedabad, Gujarat 380001, India

[IV] Research Centre for Crystalline Materials, Faculty of Science and Technology, Sunway University, 47500 Bandar Sunway, Selangor Darul Ehsan, Malaysia

Received; accepted

Keywords: Zinc / cadmium / dithiocarbamate / coordination polymer / Hirshfeld surface / crystal structure analysis / X-ray diffraction

Abstract. The crystal and molecular structures of two homoleptic morpholine-derived dithiocarbamates of zinc, binuclear $\{Zn[S_2CN(CH_2CH_2)_2O)_2]_2\}_2$ (**1**), and cadmium, one-dimensional coordination polymer $\{Cd[S_2CN(CH_2CH_2)_2O)_2]_2\}_2$ (**2**), are described. In **1**, a centrosymmetric binuclear molecule is found as there are equal numbers of chelating and bidentate bridging dithiocarbamate ligands; weak transannular Zn···S interactions are found within the resultant eight-membered $\{\cdots SCSZn\}_2$ ring which has the form of a chair. The resultant 4+1 S_5 donor set is highly distorted with the geometry tending towards a square-pyramid. By contrast, a square-planar geometry is found in centrosymmetric **2** defined by symmetrically chelating dithiocarbamate ligands. The presence of Cd···S secondary bonding in the crystal of **2** leads to a distorted 4+2 S_6 octahedron and a linear coordination polymer, which is unprecedented in the structural chemistry of cadmium dithiocarbamates. The analyses of the Hirshfeld surfaces for **1** and **2** show the dominance of H…H, S…H/H…S and O…H/H…O contacts to the surface, i.e. contributing around 90 and 80%, respectively.

* Correspondence authors: edwardt@sunway.edu.my (E.R.T.T.)

Introduction

The propensity of the homoleptic zinc-triad 1,1-dithiolates, *i.e.* xanthates ($^{-}S_2COR$), dithiophosphates [$^{-}S_2P(OR)(OR')$] and dithiocarbamates ($^{-}S_2CNRR'$), for R, R' = alkyl/aryl, to form bridges thereby leading to high nuclearity aggregates has been reviewed very recently [1]. Of the mentioned 1,1-dithiolate anions, the dithiocarbamates tend not to form extended aggregates, behaviour that is readily rationalised in terms of the significant contribution of the canonical form $^{(2-)}S_2C{=}N^{(+)}RR'$ to the overall electronic structure. With a formal negative charge on each sulphur atom, dithiocarbamates are very efficient chelators of metal atoms and reduce the Lewis acidity of the heavy elements they are coordinated to. Nevertheless, binuclear aggregates are usually formed for the homoleptic dithiocarbamates $[M(S_2CNRR')_2]_2$ for M = Zn. Cd and Hg, where there are equal numbers of bidentate bridging and chelating dithiocarbamate ligands [1]. One way to encourage supramolecular aggregation is by incorporating potential donor atoms in the 1,1-dithiolate ligands themselves [1] or by co-crystallisation of the metal dithiocarbamate with ligands with, typically, pyridyl-nitrogen donors [2].

In the relatively few instances where additional donor atoms are incorporated in the dithiocarbamate ligand [1], their participation in coordination has been observed. An example of this is found in the crystal of $\{Zn[S_2CN(CH_2CH_2)_2NMe]_2\}_n$, where the piperazine-nitrogen atom forms a bridging interaction with a neighbouring zinc atom to generate a one-dimensional, zig-zag coordination polymer and where the zinc coordination geometry is based on a NS_4 donor set [3]. Another example, this time in the structural chemistry of cadmium dithiocarbamates, is found in the crystal of $\{Cd[S_2CN(Me)(CH_2)_3NMe_2]_2\}_2$ where the tertiary amine-nitrogen bridges a centrosymmetrically-related molecule to form a binuclear aggregate and where the cadmium atom exists within a NS_4 donor set [4]. As a continuation of systematic structural studies in this area, homoleptic zinc(II) and cadmium(II) dithiocarbamates derived from morpholine are described, see Figure 1. The specific motivation for this study was to determine whether the morpholine-oxygen atom participates in supramolecular association, akin to the nitrogen-substituted organic groups cited above [2, 3]. Herein, the crystal and molecular structures of the title compounds, $\{Zn[S_2CN(CH_2CH_2)_2O]_2\}_2$ (**1**) and $\{Cd[S_2CN(CH_2CH_2)_2O]_2\}_n$ (**2**), are described along with an analysis of their calculated Hirshfeld surfaces.

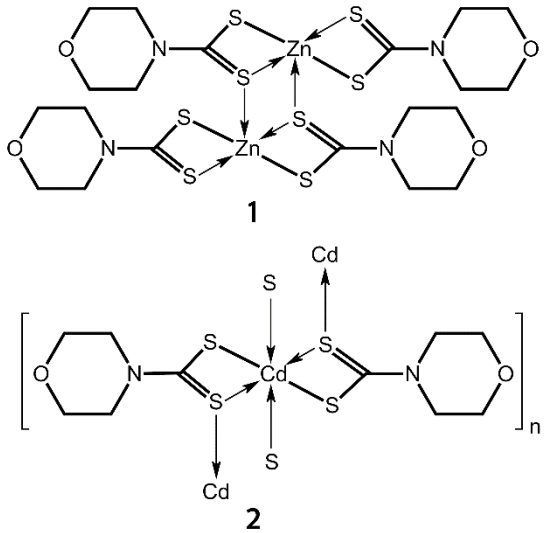

Fig. 1: Structural formula for **1** and **2**. In **2**, the Cd···S secondary bonding leading to a supramolecular polymer are indicated by arrows.

Experimental

Instrumentation

IR spectra were obtained on a Bruker Vertex 70 V spectrophotometer equipped with a Platinum ATR. ^{1}H and $^{13}C\{^{1}H\}$ NMR spectra were recorded in DMSO-d_6 solution on a Bruker Ascend 400 MHz NMR spectrometer with chemical shifts reported relative to tetramethylsilane. UV-Vis spectra were recorded in DMSO solution on a Shimadzu UV-3600 Plus spectrophotometer. The powder X-ray diffraction (PXRD) patterns were measured on a Rigaku Miniflex 600 X-ray diffractometer at 293 K using Cu Kα (λ = 1.5418 Å) radiation in the 2θ range 5 to 60°. The comparisons between experimental and calculated (from the CIF's) PXRD patterns were performed with Rigaku's PDXL2 software (https://www.rigaku.com/en/products/software/pdxl/overview).

Materials

Potassium morpholinecarbodithioate, $K[S_2CN(CH_2CH_2)_2O]$, was prepared in high yield from morpholine (Acros Organics), carbon disulphide (Panreac) and potassium hydroxide (Merck), in a 1:1:1 mole ratio, in methanol solution [5]. ^{1}H NMR (DMSO-d_6): δ 4.19 (s, 2H, -CH_2O), 3.43 (s, 2H, NCH_2) ppm. $^{13}C\{^{1}H\}$ NMR (DMSO-d_6): δ 213.8 (CS_2), 66.5 (C–O), 50.4 (C–N) ppm. The $Zn(S_2CNCH_2CH_2O)_2$ and $Cd(S_2CNCH_2CH_2O)_2$ reagents were prepared from the 2:1 reactions of $K[S_2CN(CH_2CH_2)_2O]$ with $ZnCl_2$ (Alfa Aesar) and $CdCl_2$ (Acros Organics), respectively, in methanol solution.

Synthesis

$Zn[S_2CN(CH_2CH_2)_2O]_2$ (**1**): $K[S_2CN(CH_2CH_2)_2O]$ (0.80 g, 4 mmol) in methanol (10 ml) was added slowly to $ZnCl_2$ (0.27 g, 2 mmol) also dissolved in methanol (5 ml). The resulting mixture was stirred for 60 mins at 323 K, followed by filtration. The filtrate was left for slow evaporation under ambient conditions. Colourless crystals formed after three weeks. Yield: 0.11 g (31.9%; based on Zn). M.pt: > 300 ºC. Anal. Calcd for $C_{10}H_{16}N_2O_2S_4Zn$: C 30.81; H 4.14; N 7.19. Found: C 30.93; H 4.21; N 7.11. IR (cm^{-1}): 2916 (w), 2853 (w) (C–H); 1490 (s) (C=N); 1242 (s) (C–N); 1122 (s) (C–O); 1025 (s) (C–S). ^{1}H NMR (DMSO-d_6): δ 4.03 (s, 2H, -CH_2O), 3.65 (s, 2H, NCH_2) ppm. $^{13}C\{^{1}H\}$ NMR (DMSO-d_6): δ 204.0 (CS_2), 66.1 (C–O), 51.6 (C–N). UV (nm): 224, 340 nm (π → π*).

$Cd[S_2CN(CH_2CH_2)_2O]_2$ (**2**): $K[S_2CN(CH_2CH_2)_2O]$ (0.80 g, 4 mmol) in methanol (10 ml) was added slowly to $CdCl_2$ (0.37 g, 2 mmol) also dissolved in methanol (5 ml). The resulting mixture was stirred for 60 mins at 323 K, followed by filtration. The filtrate was left for slow evaporation under ambient conditions. Colourless crystals formed after three weeks. Yield: 0.25 g (39.8%) (based on Cd). M. pt: > 300 ºC. Anal. Calcd for $C_{10}H_{16}N_2O_2S_4Cd$: C 27.49; H 3.69; N 6.41. Found: C 27.63; H 3.73; N 6.34. IR (cm^{-1}): 2968 (w), 2871 (w) (C–H); 1464 (s) (C=N); 1223 (s) (C–N); 1120 (s) (C–O); 1022 (s) (C–S). ^{1}H NMR (DMSO-d_6): δ 4.06 (s, 2H, -CH_2O), 3.64 (s, 2H, NCH_2) ppm. $^{13}C\{^{1}H\}$ NMR (DMSO-d_6): δ 202.5 (CS_2), 66.1 (C–O), 52.6 (C–N). UV (nm): 231 nm (π → π*).

Crystal structure determination

Intensity data for **1** and **2** were measured at 293 K on an Agilent Technologies SuperNova Dual diffractometer fitted with an Atlas (Mo) detector. Data collections employed Mo Kα radiation (λ = 0.71073 Å). A multi-scan absorption correction was applied in each case and data processing was accomplished with CrysAlis Pro [6]. Details of cell data, X-ray data collection, and structure refinement are given in Table 1. The structures were solved by Direct Methods [7]. Full-matrix least squares refinement on F^2 with anisotropic displacement parameters for all non-hydrogen atoms was performed [8]. The C-bound H atoms were placed on stereochemical grounds and refined with fixed geometries, each riding on a carrier atom with U_{iso} = 1.2U_{equiv}(carrier atom). A weighting scheme of the form w = 1/[$\sigma^2(F_o^2)$ + $(aP)^2$ + bP] where P = (F_o^2 + 2F_c^2)/3 was introduced in each case. In the refinement of **1**, one reflection, i.e. (0 $\bar{3}$ 1), was removed from the final cycles of refinement. The maximum and minimum residual electron density peaks of 1.18 and 0.45 eÅ^{-3}, respectively, were located 1.08 and 2.11 Å from the S2 atom, respectively. The programs WinGX [9], ORTEP-3 for Windows [9] and PLATON [10] and DIAMOND [11] were also used in the study.

Tab. 1: Crystallographic data and refinement details for **1** and **2**.[a]

	1	**2**
Formula	$C_{20}H_{32}N_4O_4S_8Zn_2$	$C_{10}H_{16}CdN_2O_2S_4$
Formula weight	779.71	436.89
Crystal colour, habit	Colourless, plate	Colourless, block
Crystal size/mm	0.02 x 0.16 x 0.20	0.08 x 0.11 x 0.12
Crystal system	triclinic	monoclinic
Space group	$P\bar{1}$	$P2_1/n$
a/Å	8.0963(12)	4.23340(10)
b/Å	8.8062(13)	11.4471(2)
c/Å	11.9454(16)	14.8477(3)
α/°	103.543(10)	90
β/°	92.099(12)	93.0670(10)
γ/°	111.316(10)	90
V/Å^3	764.4(2)	718.49(3)
Z/Z'	1/0.5	2/0.5
D_c/g cm^{-3}	1.694	2.019
F(000)	400	436
μ(Mo $K\alpha$)/mm^{-1}	2.150	2.098
Measured data	7445	6771
θ range/°	2.7 – 27.7	2.3 – 31.1
Unique data	3572	2117
R_{int}	0.066	0.027
Observed data ($I \geq 2.0\sigma(I)$)	1783	1781
R, obs. data; all data	0.072; 0.154	0.024; 0.034
a; b in wghting scheme	0.089; 0	0.021; 0.170
R_w, obs. data; all data	0.160; 0.197	0.047; 0.050
Largest difference peaks (Å^{-3})	-0.45, 1.12	-0.34, 0.40

[a] Supplementary Material: Crystallographic data (including structure factors) for the structures reported in this paper have been deposited with the Cambridge Crystallographic Data Centre as supplementary publication numbers CCDC-1871431

and 1871432. Copies of available material can be obtained free of charge, on application to CCDC, 12 Union Road, Cambridge CB2 1EZ, UK, (fax: +44-(0)1223-336033 or e-mail: deposit@ccdc.cam.ac.uk).

Results and discussion

Compounds $Zn[S_2CN(CH_2CH_2)_2O]_2$ (**1**) and $Cd[S_2CN(CH_2CH_2)_2O]_2$ (**2**) were prepared and crystallised using standard methods. A comparison of the experimental powder X-ray diffraction pattern with the simulated patterns calculated from the CIF's indicate the single crystal results are representative of the bulk materials. The most prominent observation in the collected spectroscopy is the anticipated upfield shift in the resonances due to the quaternary-C atom in each of **1** and **2**, compared with the spectrum of the free ligand, which is indicative of coordination of the ligand in DMSO-d_6 solution. Herein, a description of the crystal and molecular structures of **1** and **2** are presented followed by a more detailed analysis of the molecular packing through an evaluation of the calculated Hirshfeld surfaces.

Molecular structures

The molecular structure of centrosymmetric and binuclear $\{Zn[S_2CN(CH_2CH_2)_2O]_2\}_2$ (**1**) is shown in Figure 1 and selected geometric parameters are collected in Table 2. One dithiocarbamate ligand is bidentate, bridging two zinc(II) centres with almost equivalent Zn–S bond lengths, i.e. $\Delta(Zn–S_{long} - Zn–S_{short}) = 0.04$ Å. This results in an eight-membered $\{–SCSZn\}_2$ core with the shape of a chair and in which the bridging S2 atom forms a transannular interaction of 3.009 (2) Å, cf. 4.02 Å being the sum of the van der Waals radii [12], to form a pseudo chelate ring. The second independent dithiocarbamate ligand is chelating in a slightly asymmetric mode with Δ (Zn–S) = 0.13 Å. Reflecting the disparity in the Zn–S bond lengths, the individual C–S bond lengths are not equivalent with the C6–S4 bond associated with the longest Zn–S4 bond being shorter than the other C–S bond lengths, the relatively large standard uncertainties notwithstanding. Considerable double bond character is evident in the short C1–N1 and C6–N2 bond lengths, consistent with the significant contribution of the $^{2-}S_2C{=}N^+RR'$ canonical form to the electronic structure of the dithiocarbamate ligand, as noted in the *Introduction*.

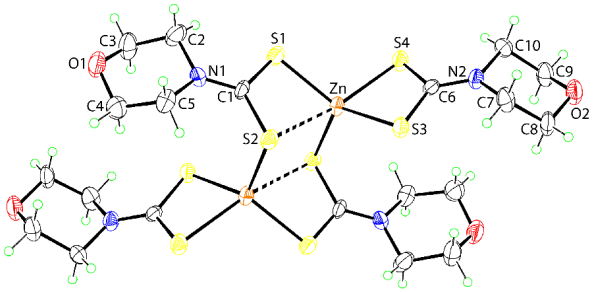

Fig. 2: The molecular structure of centrosymmetric **1**, showing atom labelling scheme and displacement ellipsoids drawn at the 35% probability level. The unlabelled atoms are related by the symmetry operation 2-*x*, 2-*y*, -*z*. The dashed lines are indicative of transannular Zn···S interactions.

Tab. 2: Selected bond lengths (Å) for **1** and **2**.

	1 (M = Zn)	**2** (M = Cd)
M–S1	2.308(2)	2.6126(5)

M–S2	3.009(2)	2.6215(4)
M–S3	2.329(2)	
M–S4	2.455(2)	
M···S2^{i}	2.352(2)	3.0559(4)
C1–S1, S2	1.748(8), 1.738(7)	1.7229(18), 1.7437(19)
C6–S3, S4	1.740(7), 1.719(7)	
C1–N1, C6–N2	1.310(9); 1.321(9)	1.330(2)
Symmetry operation i	2-*x*, 2-*y*, -*z*	-1+*x*, *y*, *z*

The range of tetrahedral angles spans over 50°, *i.e.* 76.06 (7)°, for the S3–Zn–S4 chelate angle, to 131.03 (9)°, for S1–Zn–S3, being subtended by the sulphur atoms forming the shortest bonds. The close approach of the S2 atom forming the transannular interaction, mentioned above, is partly responsible for the distortion. If the 4+1 S_5 donor set is analysed employing the five-coordinate geometry index, τ, which computes to 0.0 and 1.0 for ideal square-pyramidal and trigonal bipyramidal geometries, respectively [13], a value 0.38 is calculated, underscoring the distortion in the coordination geometry. The morpholine substituents adopt chair conformations.

The crystallographic asymmetric unit of **2** comprises half a molecule of $Cd[S_2CN(CH_2CH_2)_2O]_2$ as the cadmium(II) atom is located on a centre of inversion, Figure 3. The coordination geometry is defined by four sulphur atoms derived from a symmetrically chelating dithiocarbamate ligand with $\Delta(Cd–S_{long} - Cd–S_{short}) = 0.01$ Å, Table 2.

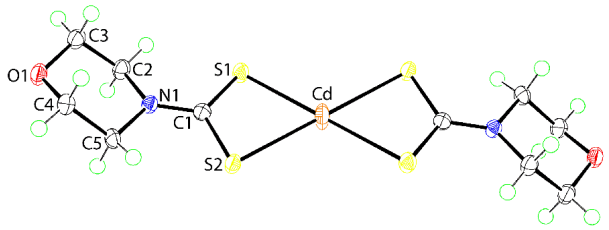

Fig. 3: Molecular structure of **2**, showing atom labelling scheme and displacement ellipsoids drawn at the 35% probability level. The molecule is disposed about a centre of inversion with unlabelled atoms related by symmetry operation -*x*, -*y*, -*z*.

The molecule self-associates via Cd···S2 interactions above and below the S_4 plane to form a linear coordination polymer orientated along the *a*-axis direction, Figure 3. The Cd···S2 separations of 3.0559 (4) Å are less than the sum of the van der Waals radii of cadmium and sulphur of 3.38 Å [12] and must be considered as significant secondary bonding interactions [14-16]. The coordination geometry is best described as 4+2 S_6, axially distorted octahedral. As for **1**, a chair conformation is noted for the independent morpholine substituent.

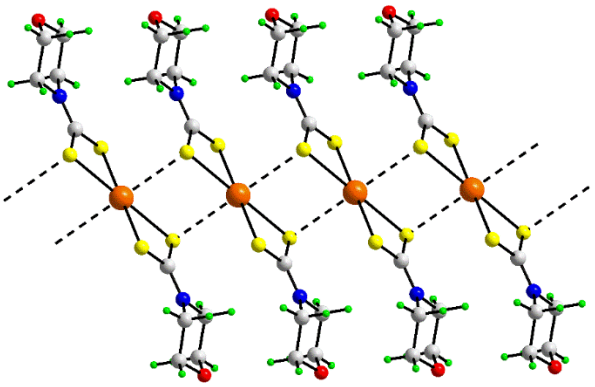

Fig. 4: A view of the linear one-dimensional coordination polymer in the crystal of **2** sustained by Cd···S secondary bonding interactions shown as black dashed lines.

As mentioned in the *Introduction*, the structural chemistry of the zinc-triad element 1,1-dithiolates has been reviewed very recently [1]. For the homoleptic zinc dithiocarbamates, $Zn(S_2CNRR')_2$, where there are no potential donor atoms in the organic substituents, there are two structural motifs: monomeric with distorted S_4 tetrahedral geometries and binuclear structures as described for **1** above. The adoption of one motif over another is ascribed to steric effects as exemplified in the structure of monomeric $Zn(S_2CNCy_2)_2$ with bulky cyclohexyl (Cy) groups [17]. Binuclear species related to **1** are usually adopted by the homoleptic cadmium dithiocarbamates as well. However, recently, one-dimensional polymeric forms have been found for $Cd(S_2CNRR')_2$ with distorted octahedral S_6 coordination geometries as each of the dithiocarbamate ligands adopts a $\mu_2\kappa^3$-coordination mode similar to the bridging ligand found in **1**. The polymers are either propagated by 2-fold symmetry, as exemplified in the crystal of the R = R' = Me species [18], or by inversion symmetry, as in the case when R = *i*-Pr and R' = CH_2CH_2OH [19]. That there are likely small energy differences between the symmetry adopted by these supramolecular polymers, i.e. with 2-fold or inversion symmetry, is evidenced in that the last mentioned species with R = *i*-Pr and R' = CH_2CH_2OH also exists in a supramolecular isomeric form with 2-fold symmetry [20]. It is noteworthy that both of the R = *i*-Pr and R' = CH_2CH_2OH structures were found to convert to the dimeric form, analogous to binuclear **1**, with time, suggesting the dimeric motif is the thermodynamic outcome of the crystallisation of these species. Being a linear, one-dimensional coordination polymer, **2** is different from the aforementioned polymers and represents a new structural motif for the homoleptic cadmium dithiocarbamates. While there are no direct precedents for the structure of **2** among the homoleptic cadmium dithiocarbamates, there are two examples of cadmium xanthates, *i.e.* $Cd(S_2COR)_2$, adopting this motif, i.e. for R = Me [21] and R = CH_2CH_2OMe [22].

From the above, it is evident that steric effects can greatly influence the aggregate found in the solid-state. Also important are kinetic versus thermodynamic effects. However, these influences are generally retrospective in that they are employed to rationalise crystallisation outcomes of homoleptic compounds rather than being predictive.

Molecular packing

The geometric parameters characterising the intermolecular interactions operating in the crystal structures of **1** and **2** are collected in Table 3. In the crystal of **1**, supramolecular layers parallel to (0 1 1) are sustained by methylene-C2–H···S3(dithiocarbamate) and methylene-C10–

H···O2(morpholine) interactions, as illustrated in Figure 5a. The connections between the layers are weak methylene-C2–H···S3(dithiocarbamate) contacts, Figure 5b.

Tab. 3: Summary of intermolecular contacts (A–H···B; Å, º) found in the crystals of **1** and **2**.

A	H	B	H···B	A···B	A–H···B	Symmetry operation
1						
C2	H2b	S3	2.79	3.703(11)	158	1-*x*, 2-*y*, -*z*
C10	H10a	O2	2.57	3.543(12)	177	1-*x*, 1-*y*, 1-*z*
C2	H2a	S3	2.96	3.650(8)	129	*x*, 1+*y*, *z*
2						
C4	H4a	O1	2.71	3.332(2)	121	2-*x*, -*y*, 1-*z*
C4	H4b	O1	2.66	3.260(2)	120	1-*x*, -*y*, 1-*z*

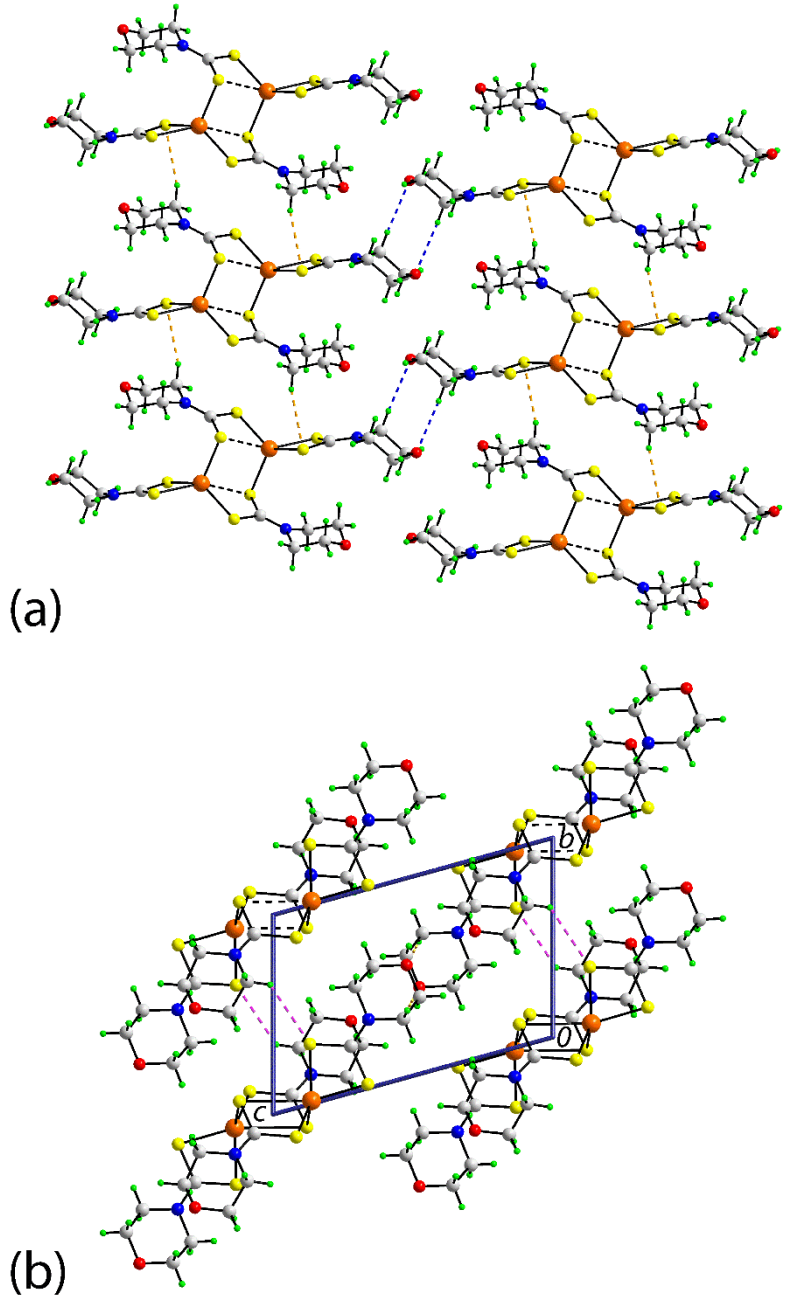

Fig. 5: Molecular packing in **1**: (a) supramolecular layer parallel to (0 1 1) sustained by methylene-C2–H···S3(dithiocarbamate) and methylene-C10–H···O2(morpholine) interactions shown as orange and blue dashed lines, respectively, and (b) a view of the unit cell contents shown in projection down the *a*-axis. The weak methylene-C2–H···S3(dithiocarbamate) interactions between layers are shown as pink dashed lines.

Supramolecular layers are also found in the crystal of **2** whereby the supramolecular chains sustained by secondary bonding are linked *via* weak methylene-C4–H···O1(morpholine) contacts, Figure 6a. Layers are formed parallel to (1 0 1) and stack along (0 1 0) with no directional interactions between them, Figure 6b.

In order to evaluate the features of the supramolecular assemblies of **1** and **2** further, an analysis of the calculated Hirshfeld surfaces was undertaken.

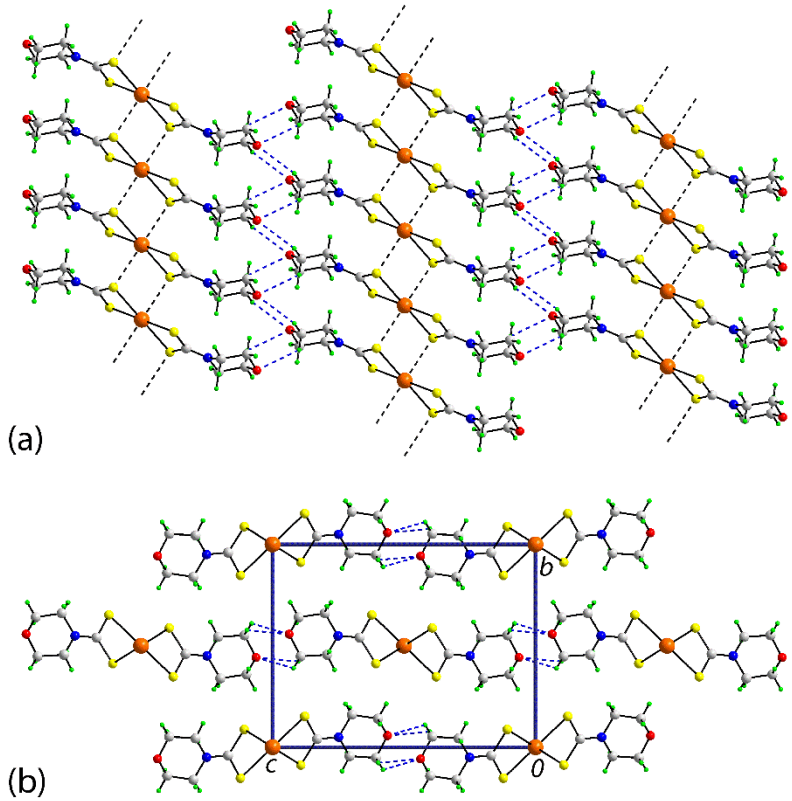

Fig. 6: Molecular packing in **2**: (a) supramolecular layer parallel to (1 0 1) sustained by methylene-C4–H···O1(morpholine) interactions shown as blue dashed lines and (b) view of the unit cell contents shown in projection down the *a*-axis showing the stacking of layers.

Hirshfeld surface analysis

The Hirshfeld surface calculations [23, 24] were performed in accord with recent studies [25], including on related zinc-triad dithiocarbamate structures [26], in order to gain a greater understanding of the molecular packing in **1** and **2**, in particular the nature of interlayer contacts.

The initial analysis revolves around the calculated three-dimensional Hirshfeld surfaces. This provides a facile approach to enable the visual comparison of intermolecular contacts relative to van der Waals radii. Thus, through a red-white-blue colour scheme [24], significant contacts, i.e. less than the sum of the respective van der Waals radii, appear red on the Hirshfeld surface mapped over d_{norm}. The blue shading is associated with longer contacts, whereas contacts at the van der Waals separation are represented by the white regions. In the case of **1**, the presence of bright-red spots near the methylene-H2b and H10a, morpholine-O2 and dithiocarbamate-S3 atoms on the Hirshfeld surface mapped over d_{norm} in Figure 7a indicate the intermolecular C–H···S and C–H···O interactions giving rise to the supramolecular layer, Table 3. Short interatomic Zn···H2b and S1···H8a contacts, as summarised in Table 4 (calculated using Crystal Explorer [24]), are also evident with the former being indicative of a weak C–H···π(chelate) interaction involving the (Zn/S3/C6/S4) ring, as the π-acceptor, and methylene-C2–H2b as the donor. This interaction is highlighted in Figure 7b and data are given in Table 5. Contacts of type C–H···π(chelate ring) are well established and were in fact probably first discussed explicitly in the structures of related cadmium 1,1-dithiolate compounds, e.g. $Cd(S_2COCH_2CH_2OMe)_2$(2,2'-bipyridyl) [27]. Such interactions are apparent in many transition metal complexes, e.g. those of sterically unencumbered acetylacetonates [28], and owing to the significant aromaticity in

chelate rings formed by dithiocarbamate ligands, are prevalent in the structural chemistry of metal dithiocarbamates [29], including those of zinc and cadmium [26, 30]. This prevalence is ascribed to the significant contribution of the $^{(2-)}S_2C{=}N^{(+)}RR'$ canonical form to the overall electronic structure of dithiocarbamate anions as discussed above. An estimate, based on DFT calculations on $Pd(S_2CO\text{-}n\text{-}Pr)_2$, of the energy of stabilisation provided by a C–H···π(PdS_2C) interaction is 62.9 kJ mol^{-1} [31], which was found to be comparable to a cooperative Pd···S contact in the same structure and indeed, conventional hydrogen bonding interactions [16].

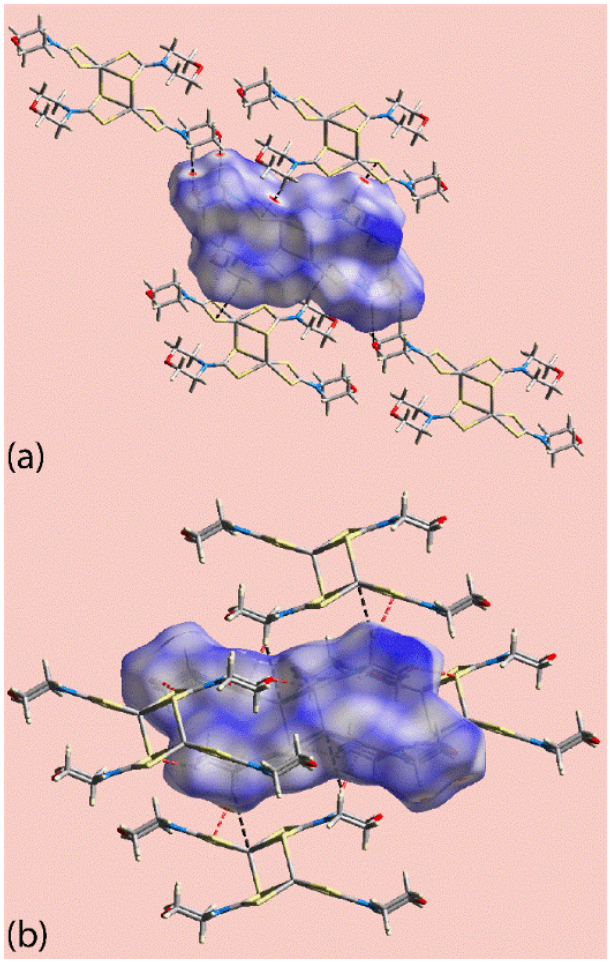

Fig. 7: Views of Hirshfeld surfaces mapped over d_{norm} for **1**, mapped over the range -0.149 to +1.526 atomic units (a.u.) and highlighting (a) intermolecular C–H···S and C–H···O interactions, shown as black dashed lines, and (b) short interatomic S···H and Zn···H contacts shown by red and black dashed lines, respectively. The brightest spots correlate with the most significant intermolecular interactions.

Tab. 4: Additional short inter-atomic contacts (Å) in the crystals of **1** and **2**.

Contact	Distance (Å)	Symmetry operation
1		
Zn···H2b	3.22	1-*x*, 2-*y*, -*z*
S1···H8a	2.93	*x*, 1+*y*, *z*
2		
H2a···H5a	2.14	1½ -*x*, -½+*y*, ½-*z*
O1···O1	3.2209(18)	2-*x*, -*y*, 1-*z*
O1…H3a	2.54	1+x, y, z
N1···H5b	2.69	-1+*x*, *y*, *z*
C1···H5b	2.71	-1+*x*, *y*, *z*

On the Hirshfeld surface mapped over d_{norm} for **2**, Figure 8a, the broad, bright-red-spots near the Cd and S2 atoms result from the Cd···S secondary bonding interactions leading to the supramolecular chain shown in Figure 3. The short inter-chain C–H···O, N···H and C···H contacts, Table 4, appear as the diminutive-red spots near the respective atoms in Figure 8a. The aforementioned Cd···S and weak interactions are also evident in Figure 8b, as this, in essence, is a plan view of Figure 8a. The short intra-layer O···O and H···H contacts, summarised in Table 4, are highlighted in Figure 8b. As for **1**, the chelate rings in the crystal of **2** are also involved in the molecular packing by participating in π···π stacking interactions, as summarised in Table 5 and illustrated in Figure 8c. As with C–H···π(chelate ring) interactions, such π-stacking interactions are well established in coordination chemistry and theoretical studies indicate they can impart energies of stabilisation to the molecular packing exceeding those imparted by conventional hydrogen bonding interactions [16, 32].

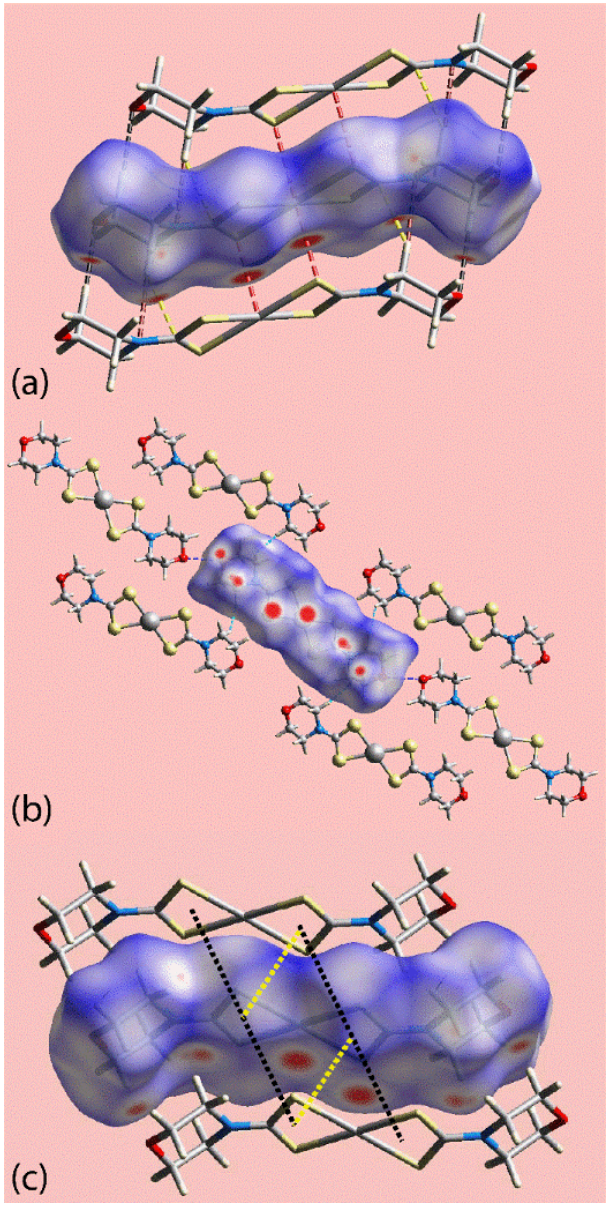

Fig. 8: Views of Hirshfeld surfaces mapped over d_{norm} for **2**, mapped over the range -0.124 to +1.526 a.u. and highlighting (a) intermolecular Cd···S secondary bonding shown with red dashed lines, and C–H···O, C···H and N···H contacts indicated by black, yellow and brown dashed lines, respectively, (b) short interatomic H···H and O···O contacts by sky-blue and blue dashed lines, respectively, and (c) π···π stacking interactions between (Cd/S1/C1/S2) chelate rings by black and yellow dotted lines, respectively. From symmetry, each chelate ring participates in two such interactions.

The donors and acceptors of intermolecular interactions in the crystals of **1** and **2** are also highlighted with blue and red regions, corresponding to positive and negative electrostatic potentials, respectively, on the Hirshfeld surfaces mapped over the calculated electrostatic potentials [33, 34] in Figure 9.

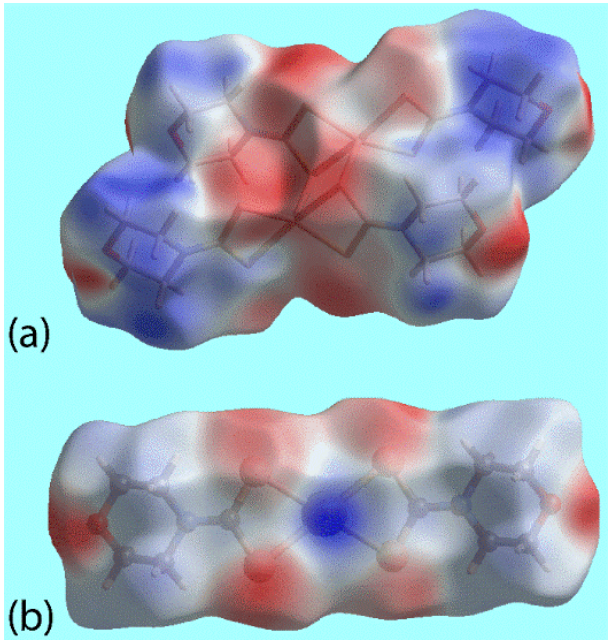

Fig. 9: Views of the Hirshfeld surface mapped over the calculated electrostatic potential for (a) **1**, mapped over the range -0.049 to +0.045 a.u., and (b) **2**, mapped over the range -0.057 to +0.132 a.u. The red and blue regions represent negative and positive electrostatic potentials, respectively.

The overall two-dimensional fingerprint plots for **1** and **2** are presented in Figure 10a, and fingerprint plots focussing on pairwise interactions, i.e. H···H, O···H/H···O, S···H/H···S and M···H/H···M for **1** and **2**, and for **2** only C···H/H···C (upper view) and N···H/H···N contacts [35], are illustrated in Figures 10b-f, respectively; the percentage contributions from the different interatomic contacts to their Hirshfeld surfaces are summarised in Table 6. The fingerprint plots are derived by plotting the fraction of points on the Hirshfeld surface as a function of (d_i, d_e), where d_e and d_i represent the distances from a point on the surface to the nearest atoms outside and inside, respectively. In the images of Figure 10, the points are coloured as a function of the number of surface points. The highest fraction of points is indicated by red, blue corresponds to relatively few points and, finally, green indicates a moderate fraction of points [36].

Tab. 6: Percentage contributions of various intermolecular contacts to the Hirshfeld surfaces of **1** and **2**.

Contact	Percentage contribution	
	1 (M = Zn)	**2** (M = Cd)
H···H	40.7	37.9
O···H/H···O	12.0	10.2
S···H/H···S	39.7	31.2
N···H/H···N	0.0	1.9
C···H/H···C	2.2	3.7
C···O/O···C	0.6	0.0
C···S/S···C	1.8	2.6
O···O	0.7	0.5
N···O/O···N	0.8	0.0
N···S/S···N	0.5	0.8
S···S	0.0	2.7
M···H/H···M	1.1	1.3
M···S/S···M	0.0	5.9
M···C/C···M	0.0	1.3

Tab. 5: Summary of weak intermolecular contacts (A–H···B; Å, º) found in the crystals of **1** and **2**.

A	H	B	H···B	A···B	A–H···B	Symmetry operation
1						
C2	H2b	Cg(Zn/S3/C6/S4)	2.92	3.836(11)	158	1-*x*, 2-*y*, -*z*
2						
Cg(Cd/S1/C1/S2)	–	Cg(Cd/S1/C1/S2)^{i}	–	3.7140(1)	0	1-*x*, *y*, z

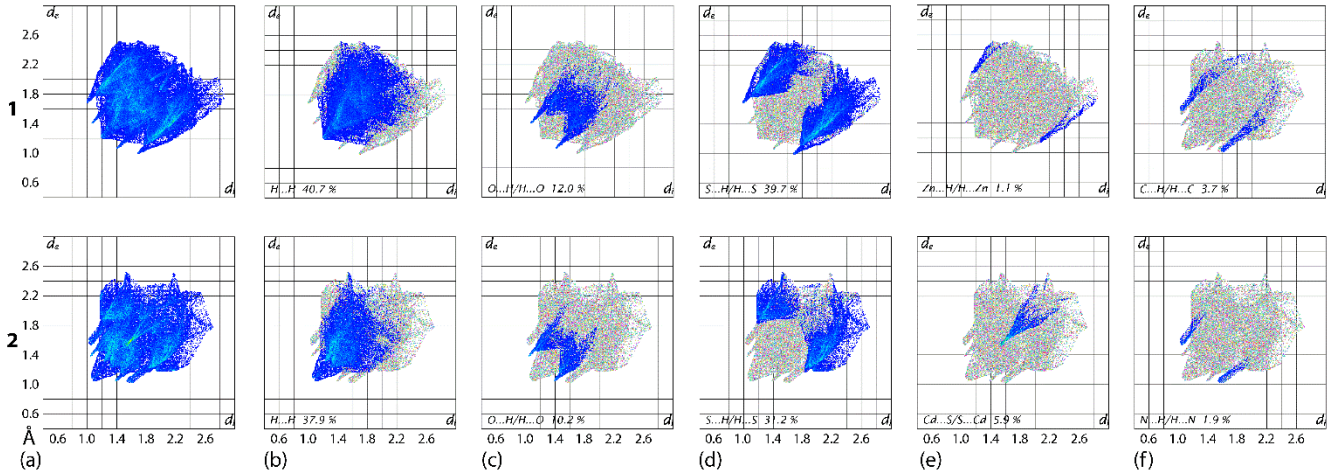

Fig. 10: Fingerprint plots calculated for **1** (upper plots) and **2**: (a) overall plots, and plots delineated into (b) H···H, (c) O···H/H···O, (d) S···H/H···S, (e) M···H/H···M and (f) specifically for **2**: C···H/H···C (upper view) and N···H/H···N (lower) contacts.

The fingerprint plots delineated into H···H contacts of Figure 10b show only van der Waals contacts for the hydrogen atoms of **1**. By contrast, in **2** a single parabolic tip at de + di ~ 2.2 Å is indicative of short intra-layer H···H contacts, listed in Table 4 and illustrated in Figure 8b. The presence of intermolecular methylene-C10–H···O2(morpholine) and methylene-C4–H···O1(morpholine) interactions in **1** and **2**, respectively, are characterised as the pairs of short spikes at de + di ~ 2.5 Å in Figure 10c. Further, the weak methylene-C–H···O1(morpholine) contacts in **2**, Table 4, are evident as the pair of conical tips at de + di ~ 2.7 Å.

The interatomic S···H/H···S contacts, making second largest percentage contributions to the Hirshfeld surfaces, Table 6, arise as a result of the involvement of dithiocarbamate-S atoms in C–H···S interactions, as discussed above. For **1**, these interactions are reflected as the pair of forceps-like tip at de + di ~ 2.8 Å superimposed upon the pair of conical tips at de + di ~ 3.0 Å, Figure 10d. The pair of finger tips at de + di ~ 3.2 Å in the fingerprint plot delineated into Zn···H/H···Zn contacts, Figure 10e, together with the aforementioned short interatomic S···H/H···S contacts, confirm the presence of the C–H···π(chelate ring) interactions, Table 5, in the crystal of **1**. The secondary bonding interactions of the form Cd···S2 in **2** are also evident as the pencil-like tip de + di ~ 3.0 Å in the fingerprint plot delineated into Cd···S/S···Cd contacts, Figure 10e. The pairs of finger tips at de + di ~ 2.7 Å in the fingerprint plots delineated into C···H/H···C (upper view) and N···H/H···N contacts in Figure 10f also show the influence of the weak inter-layer short contacts in the packing of **2**.

Conclusions

While the binuclear structure of **1** conforms to expectation, a new structural motif for the homoleptic cadmium(II) dithiocarbamates is revealed for **2** in the present study, in the form of a linear, one-dimensional coordination polymer. Such a discovery underscores the importance of systematic crystallographic studies, including polymorph screening, in order to fully understand the structural chemistry main group element 1,1-dithiolates, which are well known to be dependent on the nature of the remote organic substituent(s).

Acknowledgments: We thank Sunway University for support of crystal engineering studies of metal 1,1-dithiolates.

References

[1] E. R. T. Tiekink, *Crystals* **2018**, *8*, article no. 18.
[2] E. R. T. Tiekink, *Crystals* **2018**, *8*, article no. 292.
[3] S. N. A. Halim, Personal communication to the Cambridge Structural Database, **2015**. Refcode: QUQTED
[4] W. Clegg, R. A. Coxall, Personal communication to the Cambridge Structural Database, **2016**. Refcode: OJEQUR.
[5] A. C. Mafud, *Acta Crystallogr. E* **2012**, *66*, m1025.
[6] CrysAlis PRO, Rigaku Oxford Diffraction, Yarnton, Oxfordshire, England, 2014.
[7] G. M. Sheldrick, *Acta Crystallogr. A* **2008**, *64*, 112.
[8] G. M. Sheldrick, *Acta Crystallogr. C* **2015**, *71*, 3.
[9] L. J. Farrugia, *J. Appl. Crystallogr.* **2012**, *45*, 849.
[10] A. L. Spek, *J. Appl. Crystallogr.* **2003**, *36*, 7.
[11] K. Brandenburg, DIAMOND. Crystal Impact GbR, Bonn, Germany, **2006**.
[12] A. Bondi, *J. Phys. Chem.* **1964**, *68*, 441.

[13] A. W. Addison, T. N. Rao, J. Reedijk, J. van Rijn, G. C. Verschoor, *J. Chem. Soc. Dalton Trans*. **1984**, 1349.
[14] N. W. Alcock, *Adv. Inorg. Chem. Radiochem*., **1972**, *15*, 1.
[15] I. Haiduc, *Secondary Bonding* in J. L. Atwood, J. Steed, (Eds), *Encyclopedia of Supramolecular Chemistry*, Marcel Dekker Inc., New York, **2004**, pp. 1215.
[16] E. R. T. Tiekink, *Coord. Chem. Rev*. **2017**, *345*, 209.
[17] M.J. Cox, E. R. T. Tiekink, *Z. Kristallogr*. **1999**, *214*, 184.
[18] Y. Bing, X. Li, M. Zha, Y. Lu, (2010). *Acta Crystallogr. E* **2010**, *66*, m1500.
[19] Y. S. Tan, A. L. Sudlow, K. C. Molloy, Y. Morishima, K. Fujisawa, W. J. Jackson, W. Henderson, S. N. Bt. A. Halim, S. W. Ng, E. R. T. Tiekink, *Cryst. Growth Des.* **2013**, *13*, 3046.
[20] Y. S. Tan, S. N. A. Halim, E. R. T. Tiekink, *Z. Kristallogr. – Cryst. Mat*. **2016**, *231*, 113.
[21] V. G. Jr. Young, E. R. T. Tiekink, *Acta Crystallogr. E* **2002**, *58*, m537.
[22] B. F. Abrahams, B. F. Hoskins, E. R. T. Tiekink, G. Winter, *Aust. J. Chem*. **1988**, *41*, 1117.
[23] J. J. McKinnon, M. A. Spackman, A. S. Mitchell, *Acta Crystallogr. B* **2004**, *60*, 627.
[24] M. J. Turner, J. J. McKinnon, S. K. Wolff, D. J. Grimwood, P. R. Spackman, D. Jayatilaka and M. A. Spackman, CrystalExplorer17, University of Western Australia, The Nedlands, Western Australia, **2017**.
[25] M. M. Jotani, J. L. Wardell, E. R. T. Tiekink, *Z. Kristallogr. – Cryst. Mat*. https://doi.org/10.1515/zkri-2018-2101
[26] M. M. Jotani, P. Poplaukhin, H. D. Arman, E. R. T. Tiekink, *Z. Kristallogr. – Cryst. Mat*. **2017**, *232*, 287.
[27] D. Chen, C. S. Lai, E. R. T. Tiekink, *Z. Kristallogr*. **2003**, *218*, 747.
[28] M. K. Milčič, V. B. Medaković, D. N. Sredojević, N. O. Juranić, Z. D. Tomić and S. D. Zarić, *Inorg. Chem*. **2006**, *45*, 4755.
[29] E. R. T. Tiekink, J. Zukerman-Schpector, *Chem. Commun*. **2011**, *47*, 6623.
[30] M. M. Jotani, Y. S. Tan, E. R. T. Tiekink, *Z. Kristallogr.* **2016**, *231*, 403.
[31] Y. S. Tan, S. N. A. Halim, K. C. Molloy, A. L. Sudlow, A. Otero-de-la-Roza, E. R. T. Tiekink, *CrystEngComm* **2016**, *18*, 1105.
[32] Dušan P. Malenov, Goran V. Janjić, Vesna B. Medaković, Michael B. Hall, Snežana D. Zarić, *Coord. Chem. Rev*. **2017**, *345*, 318.
[33] M. A. Spackman, J. J. McKinnon, D. Jayatilaka, *CrystEngComm* **2008**, *10*, 377.
[34] D. Jayatilaka, D. J. Grimwood, A. Lee, A. Lemay, A. J. Russel, C. Taylo, S. K. Wolff, C. Chenai, A. Whitton, TONTO – A System for Computational Chemistry, **2005**.
[35] J. J. McKinnon, D. Jayatilaka, M. A. Spackman, *Chem. Commun*. **2007**, 3814.
[36] A. L. Rohl, M. Moret, W. Kaminsky, K. Claborn, J. J. Mackinnon, B. Kahr, *Cryst. Growth Des*. **2008**, *8*, 4517.